Blood Flow Measurement Using Variable Velocity Encoding in the RR Interval

Michael H. Buonocore

Velocity-encoded phase imaging using asynchronous gating requires input of a velocity encoding value to set the velocity sensitivity of the pulse sequence. The raw data interpolation and reconstruction scheme that the pulse sequence uses forces the encoding value to be constant throughout the RR interval. The sequence and the raw data interpolation scheme were modified to allow two velocity encodings during the RR interval. Two-hundred cm/s encoding was used in systole, and 30 cm/s in diastole. Changing the encoding in diastole significantly improved the accuracy and precision of ascending aorta flow measurements.

Key words: pulse sequences; flow measurement; phase contrast; variable velocity encoding.

INTRODUCTION

Velocity encoded phase imaging using asynchronous (also referred to as retrospective) cardiac gating (VINNIE pulse sequence, GE Medical Systems (1)) requires input of a velocity encoding value to set the velocity sensitivity. When the flow being measured is pulsatile, as in the ascending aorta, it is desirable to change the velocity encoding within the RR interval, setting a high value during systole when the flow is large, and a low value during diastole when the flow is small. However, the raw data interpolation and reconstruction scheme used in the VINNIE pulse sequence forces the encoding to be constant throughout the RR interval (2).

A previous study identified velocity encoding and three other factors as important influences on the accuracy and precision of net, forward and backward flow measurements in the mid-ascending aorta (3). Gated, velocity-encoded phase imaging with constant velocity encoding in the RR interval has been used to quantitate flow in, for example, the ventricular system (4, 5), carotid arteries (6), lungs (7), ascending aorta (8), coronary arteries (8–10), coronary venous sinus (11), cardiac ventricular chambers and valves (12–14), portal venous system (15), abdominal aorta (16), and arteries of the lower extremity (17, 18), for cardiac parameters such as stroke volume (19), and in pathological conditions such as cerebral A-V malformation (20), and chronic aortic dissection (21). This paper presents measurements using flow

phantoms and normal subjects showing the advantages of variable velocity encoding for measurement of pulsatile flow. Variable velocity encoding has recently been described in a gated line scan projection angiography pulse sequence (22). In this 1-D sequence, it improved visualization of slow flow in projection angiograms. The sequence did not use cross-sectional velocity-encoded phase images, and did not involve analysis of flow measurements derived from the projection images.

Asynchronous cardiac gating is distinguished from the more familiar synchronous gating in that in the former the playout of the sequence is not explicitly triggered by the cardiac R-wave. Asynchronously gated sequences use numerical interpolation to map encoded and nonencoded raw data to predefined time points where images are reconstructed. Raw data can be acquired late in the RR interval without the familiar 100–200 ms "dead time" to detect the trigger. Measurement of late diastolic ascending aorta flow is critically important for estimation of coronary artery flow (1).

METHODS

Measurements of midascending aorta flow using axial images were obtained in 10 normal subjects. Informed consent was obtained from all subjects. The gated VINNIE pulse sequence parameters were $TR = 33$ ms, $TE = 9$ ms, FOV = 40 cm, Flip = 30°, 128 × 256 matrix, and 200 or 30 cm/s encoding. Each scan provided 16 phase images representing 16 equally spaced time points in the average RR interval. For each subject, scans were performed in succession with 200, 30, 30, 200 cm/s encoding to provide repeated measurements. The average heart rate varied less than 3% from the average over the four scans. Nongated flow phantom studies were done to substantiate the results in normal subjects. The VINNIE pulse sequence parameters were the same except for 256 × 256 matrix, HR = 60 beats/min and FOV = 20 cm in Study #1877, FOV = 40 cm in Study #1878. In each of the two studies, four scans were performed in succession with 200, 30, 30, 200 cm/s encoding at each of two different flow rates. Sixteen scans of the flow phantom were done, with each providing 16 images. Two additional sets of flow experiments were done to confirm significant qualitative features of the images.

The VINNIE sequence and its raw data interpolation scheme were modified to allow two velocity encodings within the RR interval. Two-hundred cm/s velocity encoding was used in systole, and 30 cm/s in diastole (remainder of RR interval). This transition is represented in Fig. 1. The transition was set to the first nonencoded data acquisition before 50% into the average RR interval. Velocity encoded and non-encoded raw data was collected in alternate TR intervals. These were interpolated to time

FIG. 1. Top: Typical flow profile from the midascending aorta showing net, forward, and backward velocities. The values shown are averages over the entire aorta; they are not peak velocities. Forward and backward are defined as pixel values greater or less than the zero velocity (background) value, respectively, determined from ROIs on the lateral chest wall, Middle: In each *TR* interval, data acquisition occurs at a specific encoding. The sequence alternates between encoded and nonencoded data acquisition. The higher encoding occurs in systole. The lower encoding occurs after a present number of *TR* intervals selected as part of scan setup. Data acquisition timing runs independently of the EKG trigger, so in general the first data acquisition occurs at different times within the first *TR* after the trigger, Bottom: Raw data is interpolated to time points defined as fractions of the RR interval. Encoded and nonencoded raw data are interpolated independently. Sixteen equally spaced time points for image reconstruction are shown. The arrow lengths are proportional (conversely) to the relative weighting of the data in the interpolation formula. Interpolation between data having different encoding is blocked in the new interpolation scheme.
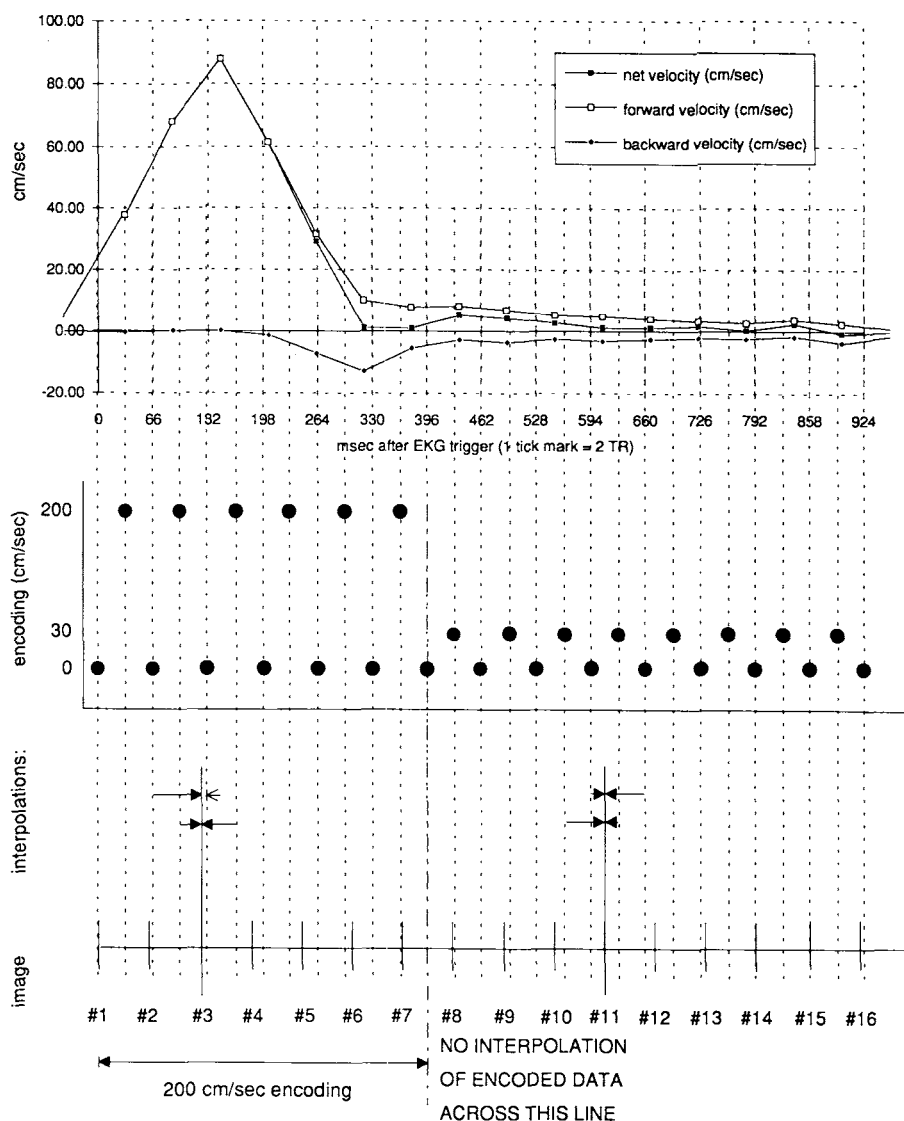
points defined by fixed percentages of each RR interval. When the velocity encoding is constant through the RR interval, linear interpolation can be applied throughout the RR interval (23). A new interpolation scheme for variable velocity encoding was written that prevented linear interpolation across the encoding transition for the encoded data and provided, when needed, raw data extrapolation to image time points near the transition.

Flow through the phantom (see Fig. 2) was driven by a peristaltic pump (Cole-Parmer, Inc.) providing average flow rates of 1240 cc/min and 885 cc/min for the two rates used in the experiments. The flow was measured by recording the time to fill a two-liter graduated cylinder. Fluid was collected over 90 and 135 s, respectively, and each measurement had an accuracy of about ±0.25% standard deviation. The measurements were performed throughout scanning at approximately 4-min intervals, and the mean flow and linear variation during each scan were determined by interpolation. Flow was computed by summation over the tube region of the velocity times the pixel area.

Flow measurements using 200 cm/s versus 30 cm/s

encoding were compared with respect to 1) reproducibility (precision), and 2) differences between means. The phantom results were also compared directly to the physical flow measurement. Statistical analysis of the normal subject measurements consisted of pairwise t tests and F tests for comparisons across subjects of net, forward and backward flow means and standard deviations. Comparison was limited to the diastolic images, i.e., those for which the 30 cm/s images did not have velocity induced phase-wraparound. Statistical analysis of the tube measurements assumed that variations of the flow measurement in different images from the same scan were statistical and due to the random fluctuation of the flow relative to data acquisition. Pair-wise t tests and F tests across subjects for comparison of means and standard deviations were done for each tube using velocity encoding as the main effect.

RESULTS

The differences between 200 cm/s encoding and 30 cm/s encoding are apparent in the two diastolic images of Fig.
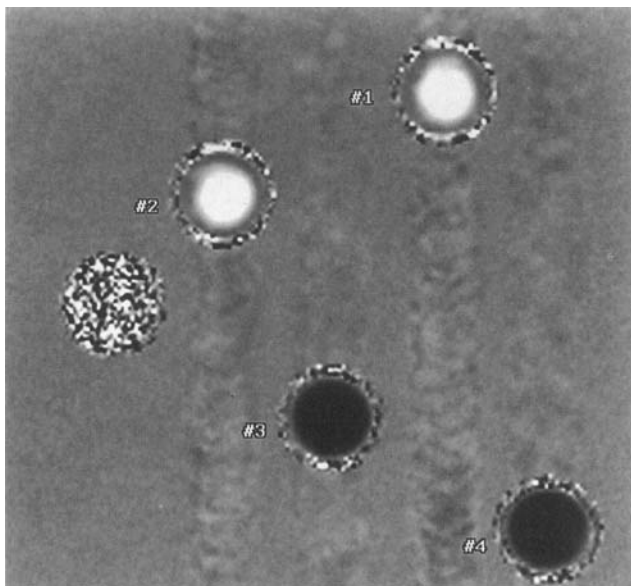
FIG. 2. Axial image through flow phantom consisting of four parallel tubes of 3/4-inch internal diameter carrying doped water (MnCl$_2$, T_1 = 700 ms) in either the S → I or I → S direction. Flow was in a single continuous lumen passing back and forth through the slice in the order #1 → #3 → #2 → #4. The phantom had 18 inches of straight, constant diameter tubing on both sides of the imaged slice to promote nonturbulent flow. Tubes #1 and #2 are white indicating flow in the same direction as the backward flow in the ascending aorta in the normal subjects. Tubes #3 and #4 flow is in the same direction as ascending aorta forward flow. Surrounding the tubes was MnCl$_2$-doped water with T_1 = 600 ms approximately.

3. Figure 4A shows typical mean and standard deviations of net flow measurements at the two encodings. Similarly, Figure 4B shows the backward flow. Error bars illustrate that measurements obtained with 200 cm/s encoding have larger variation. Table 1a gives a statistical comparison across 10 subjects of 200 cm/s versus 30 cm/s encoding for net, backward and forward flow. The t tests show that the net and backward flow measurements at the two encodings are significantly different. The standard deviation is predominantly a reflection of the normal subject variability, and differences observed between the two encodings were not significant. This table shows that the average net flow in diastole was 103.2 cc/min with 200 cm/s encoding and 625.2 cc/min with 30 cm/s encoding. This difference occurs in images 8 through 16 (last 56.25% of RR interval), therefore, the net flow difference for the entire cardiac cycle was 522 × 0.5625 = 293.6 cc/min, or about 5.9% of normal cardiac output. Similarly, the average backward flow measurement was 722.4 cc/min with 200 cm/sec encoding and 325.5 cc/min with 30 cm/s encoding. Therefore, the backward flow difference for the entire cardiac cycle was 396.9 × 0.5625 = 223.3 cc/min, or about 27.9% of typical total backward flow. Table 1b compares the standard deviations of the flow measurements at the two encodings. The net, forward and backward flow measurement standard deviations were significantly smaller using 30 cm/s encoding compared with 200 cm/s encoding. The right col-
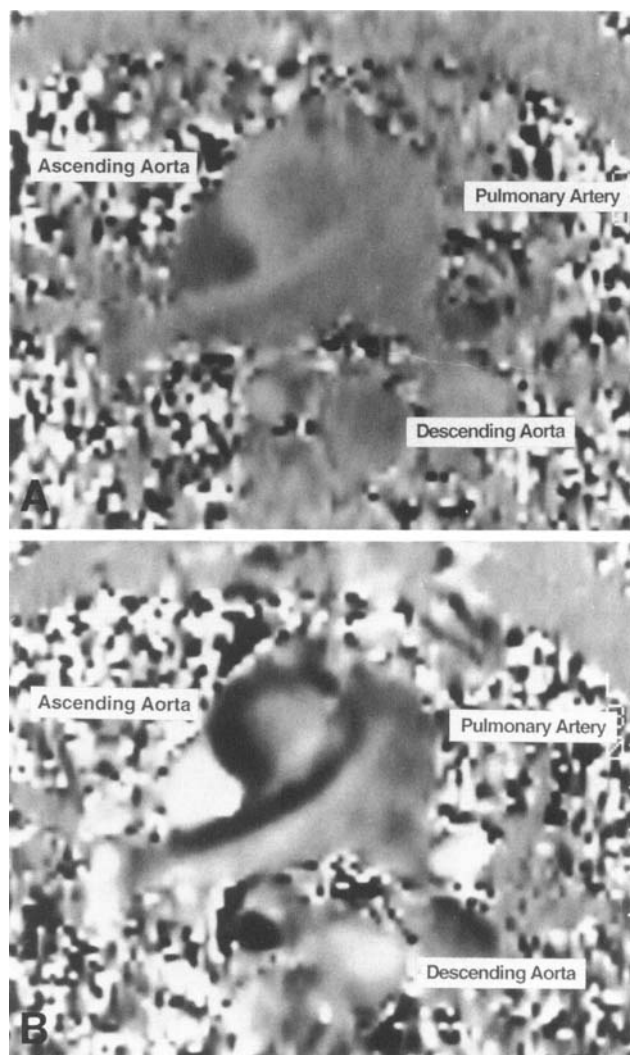

FIG. 3. Diastolic velocity encoded phase images (image 10 of 16) of the midascending aorta show the gray scale range differences using (A) 200 cm/s and (B) 30 cm/s encoding. Window and level settings are identical. Thirty cm/s encoding allows the slow flows in diastole to cover the full range of phase accumulation (±180°). This range is mapped across the entire gray scale, reflecting a corresponding wider range of numerical values and improved phase resolution.

umn shows that the variations of the standard deviations at 30 cm/s encoding were significantly less. Figure 5 shows typical measurements from the flow phantom images at 200 and 30 cm/s encoding. Flow measurements at 30 cm/s encoding are clearly more reproducible, and they are also closer to the actual flow. Table 2 shows the comparisons of mean and standard deviation for images 4 through 16 in each tube. Measured flows using 200 versus 30 cm/s encoding differed significantly in Tubes #1 and #2 (modeling backward flow). Measurements using 30 cm/s were much closer to the actual flow. These effects were the same as shown in Fig. 4 for backward flow in normal subjects. In Tubes #3 and #4, mean flow differences using the two velocity encodings were not significant. The statistics matched those of forward flow
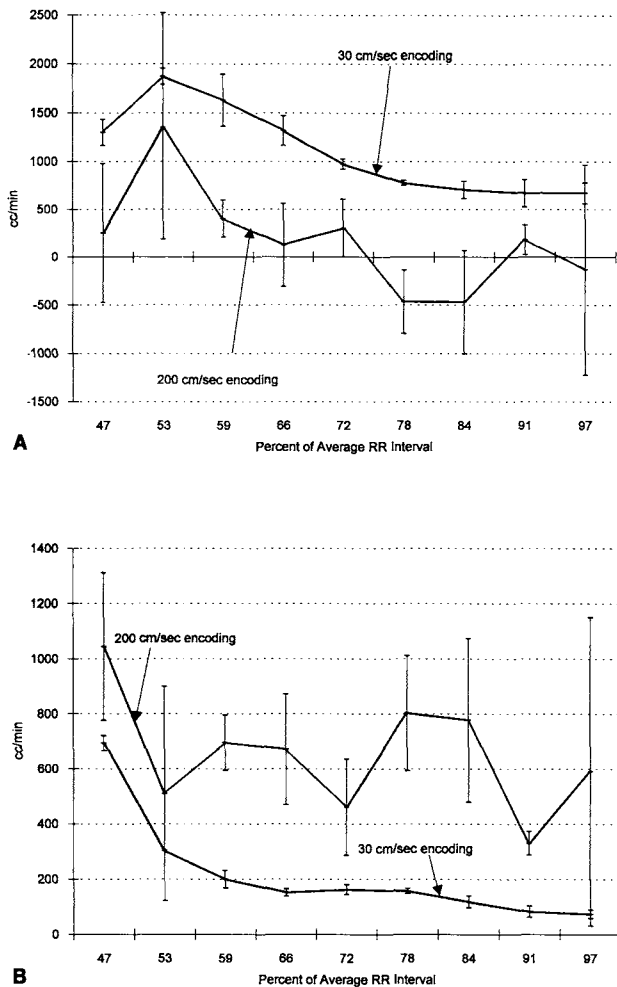
FIG. 4. Representative flow profiles computed from the diastolic (last 9 of 16) midascending aorta images obtained with 200 and 30 cm/s encoding in a normal subject. Error bars are computed from two scans at each encoding. (A) *Net flow in diastole:* Features typical of all subjects are (1) larger measurements using 30 cm/s, and (2) less measurement variation at each time point using 30 cm/s, (B) *Backward flow in diastole:* Features typical of all subjects are (1) smaller measurements using 30 cm/s, and (2) less measurement variation at each time point using 30 cm/s.

direction in normal subjects. In all tubes, flow measurements at 200 compared with 30 cm/s encoding had significantly increased standard deviation.

DISCUSSION

There are two types of error whose influence on velocity measurements are reduced with lower encoding. The first is the random variation of the spin phase. Statistics of phase measurements have been derived from the theory of system and sample noise propagation into the phase image (24–26). Improvement in phase measurements using 30 versus 200 cm/s encoding is expected. In nonpulsatile flow, the signal-to-noise ratio (SNR) of phase measurements are derived from the errors in the real-valued signals in the quadrature receiver system. It is

inversely proportional to the total signal amplitude, and independent of the accumulated phase. However, the accumulated phase is directly proportional to the spin velocity, so the SNR is expected to improve linearly with increasing velocity. The accumulated phase is *inversely* proportional to the velocity encoding value, so the SNR improves linearly with *decreasing* value. This last result predicts that the flow measurement SNR will improve in proportion to the reduction in the velocity encoding value, e.g., a reduction from 200 to 30 cm/s will improve the SNR by a factor of 6.67. However, this analysis is incomplete in that measurement errors due to beat-to-beat variation of the flow (23, 27) are not taken into account. Blood flow is not perfectly periodic so the data acquisition at each phase encode step reads a different flow profile. Image artifacts and errors due to beat-to-beat variations may be greater than those due to system and stationary sample noise. Therefore, improvement in flow measurement due to variable velocity encoding is expected to be less than that predicted by the analysis. Table 1b shows that the average standard deviation of repeated net flow measurements was 406.1 cm/s with 200 cm/s encoding, but only 119.3 cc/min with 30 cm/s encoding ($P = 0.0001$), giving a multiplicative factor of 3.40. Similarly, the average standard deviation of repeated backward flow measurements was 239.2 cc/min with 200 cm/s encoding, but only 47.8 cc/min with 30 cm/s encoding ($P = 0.0001$), giving a multiplicative factor of 5.00. With the flow phantom data, the average multiplicative factor increase in standard deviation from 30 to 200 cm/s was 4.56.

The second type of error is the phase offset remaining *after* the nonencoded phase image has been subtracted from the encoded phase image. This offset is believed to be due to differences in the eddy currents generated by the different velocity encoding gradient waveforms. It can be eliminated with an accurate pixel value representing the zero velocity (i.e., background) at the vessel location for each phase image. Errors in the background value are due to misplacement of the ROIs relative to the vessel such that the calculation does not fully compensate the background trend (3). Typical errors are ±4 pixel units unless special procedures are applied. At best, the background error can be reduced to approximately ±1 unit. With the flow phantom image, the size and placement of the ROIs was severely limited by the need to avoid placement on flow artifacts, so some errors in the background were expected. The effect of background value error on the flow measurements provides an important motivation to reduce the velocity encoding value. The flow measurement error is determined by multiplication of the background error by the encoding value, so reducing the encoding value provides a corresponding reduction in the background error's impact. For any given set of ROIs for measuring the background value, the error is expected to be 200/30 = 6.67 times greater with the 200 cm/s encoding. For example, four pixel units translates to an error in the backward flow of 31.7% at 200 cm/s, but only 4.8% at 30 cm/s. This assumes that the phase offsets, measured in pixel units, are the same at both encodings. If these offsets are significantly greater at

Table 1a
Statistics of Mean Diastolic Flow in Normal Subjects

Flow Direction	Encoding (cm/s)	Mean (cc/min)	Probability	Standard Deviation (cc/min)	Probability
Net	30	625.2		525.4	
	200	103.2	0.0029	511.6	0.9086
Forward	30	950.7		258.0	
	200	825.6	0.1971	338.4	0.2461
Backward	30	−325.5		418.9	
	200	−722.4	0.0060	442.5	0.8136

Table 1b
Statistics of Standard Deviation of Diastolic Flow in Normal Subjects

Flow Direction	Encoding (cm/s)	Mean (cc/min)	Probability	Standard Deviation (cc/min)	Probability
Net	30	119.3		96.2	
	200	406.1	0.0001	541.8	<0.0001
Forward	30	105.0		83.0	
	200	262.1	0.0001	353.3	<0.0001
Backward	30	47.8		56.4	
	200	239.2	0.0001	286.3	<0.0001

the lower encoding, the error at the lower encoding would be disproportionately higher. For example, at 200 cm/s encoding, the measured 6.68% error in the Tube #1 flow corresponded to a 2.31 pixel unit error in the background value. With 30 cm/s encoding, the measured 1.02% error in the flow corresponded to a 2.35 pixel unit error in the background value. On average in Tubes #1 and #2, the difference between the MR and physical flow measurement was 5.90 times higher using 200 cm/s encoding, rather than 6.67. This comparison illustrates that the phase offsets generated by the 30 cm/s encoding are

FIG. 5. Representative graph of repeated net flow measurements in the phantom using 200 and 30 cm/s encoding, Tube #1, study 1877. Measurements at different milliseconds after EKG trigger (labeled by image number) are regarded as independent random samples, and thus reflect the random variations of normal subject flow measurements at any particular point in time in diastole. Since tube flow is in one direction only, net flow in Tubes #1 and #2 can be compared with backward (or Tubes #3 and #4 with forward) flow in normal subjects.

only slightly greater (13%) than those generated by the 200 cm/s encoding.

The maximum velocity encoded in the VINNIE pulse sequence should be matched to the prevailing velocities. However, more levels of encoding, which would provide a tighter match to the velocities, may not be advantageous. The pulse sequence requires interpolation of the raw data in adjacent 2*TR intervals. However, variable velocity encoding precludes interpolation. Therefore, a tradeoff exists between the improved resolution of matched velocity encoding and the degradation of the images due to not being able to interpolate the data. One velocity encoding transition is probably optimal. Synchronously gated pulse sequences can be easily modified to perform variable velocity encoding. Asynchronously gated sequences are more complicated because of the need to modify the interpolation scheme. Variable velocity encoding cannot be implemented in the current Signa system software (version 4.7.9) without significant disruption of data flow.

This paper has elucidated the importance of variable velocity encoding to improve the accuracy and precision of pulsatile flow measurements. It was not possible to independently confirm the improved accuracy of the normal subject measurements with physical flow measurements. The strong matching of measurement patterns in the phantom and normal subjects suggests that the 30 cm/s encoding measurements are more accurate in normal subjects. Variable velocity encoding should be standard for measurement of pulsatile flow. The experimental data does raise some additional questions regarding the behavior of the MR system for phase encoded velocity measurement. Better understanding of subtle spin equilibrium disruptions in the VINNIE sequence due to gradient eddy currents and gradient waveform changes in successive TR intervals are needed to understand these effects fully.
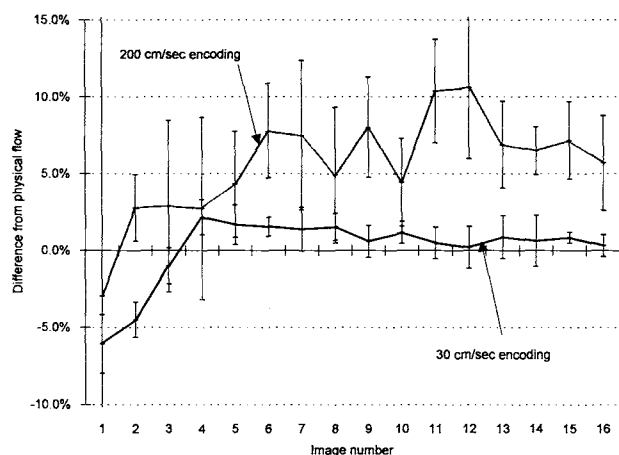
Table 2
Statistics of Flow in Tubes

Tube-study No.	Encoding (cm/s)	Mean (% from Actual)	Probability	Standard Deviation (% of mean)	Probability
1–1877	30	1.024		1.131	
	200	6.684	0.0001	3.927	<0.0001
1–1878	30	4.044		1.530	
	200	11.715	0.0001	2.743	0.0012
2–1877	30	0.794		1.376	
	200	4.236	0.0001	4.711	<0.0001
2–1878	30	1.019		1.225	
	200	6.134	0.0001	5.057	<0.0001
3–1877	30	-0.393		0.855	
	200	0.019	0.6599	4.682	<0.0001
3–1878	30	-4.460		0.542	
	200	-5.194	0.3845	4.193	<0.0001
4–1877	30	3.238		1.271	
	200	-0.716	0.0002	4.548	<0.0001
4–1878	30	-4.741		0.854	
	200	4.169	0.2070	0.667	<0.0001

REFERENCES

1. N. J. Pelc, R. J. Herfkens, A. Shimakawa, D. R. Enzmann, *Magn. Reson. Q.* **7(4),** 229 (1991).
2. M. H. Buonocore, L. Gao, H. Bogren, A. Shimakawa, *in* "Book of Abstracts, 10th Annual Meeting, Society of Magnetic Resonance, San Francisco, 1991," p. 804.
3. M. H. Buonocore, H. G. Bogren, *Magn. Reson. Med.* **26,** 141 (1992).
4. W. R. Nitz, W. G. Bradley Jr., A. S. Watanabe, R. R. Lee, B. Burgoyne, R. M. O'Sullivan, M. D. Herbst, *Radiology* **183(2),** 395 (1992).
5. D. R. Enzmann, N. J. Pelc, *Radiology* **178(2),** 467 (1991).
6. P. Bendel, E. Buonocore, A. Bockisch, M. C. Besozzi, *AJR* **152(6),** 1307 (1989).
7. G. R. Caputo, C. Kondo, T. Masui, S. J. Geraci, E. Foster, M. M. O'Sullivan, C. B. Higgins, *Radiology* **180(3),** 693 (1991).
8. S. R. Underwood, D. N. Firmin, R. S. Rees, D. B. Longmore, *Clin. Phys. Physiol. Meas.* **11**(Suppl A), 37 (1990).
9. H. G. Bogren, M. H. Buonocore, *in* "Works-in-Progress, Supplement, Society of Magnetic Resonance Imaging Annual Meeting, 1992," p. S1.
10. M. H. Buonocore, *Radiology* **185**(Suppl), 160 (1992).
11. A. C. van Rossum, F. C. Visser, M. B. Hofman, M. A. Galjee, N. Westerhof, J. Valk, *Radiology* **182(3),** 685 (1992).
12. R. H. Mohiaddin, M. Amanuma, P. J. Kilner, D. J. Pennell, C. Manzara, D. B. Longmore, *J. Comput. Assist. Tomogr.* **15(2),** 237 (1991).
13. L. Sondergaard, C. Thomsen, F. Stahlberg, E. Gymoese, K. Lindvig, P. Hildebrandt, O. Henriksen, *J. Magn. Reson. Imaging* **2(3),** 295 (1992).
14. P. J. Kilner, D. N. Firmin, R. S. Rees, J. Martinez, D. J. Pennell, R. H. Mohiaddin, S. R. Underwood, D. B. Longmore, *Radiology* **178(1),** 229 (1991).
15. C. R. Taylor, T. R. McCauley, *J. Clin. Gastroenterol.* **14(3),** 268 (1992).
16. S. E. Maier, D. Meier, P. Boesiger, U. T. Moser, A. Vieli, *Radiology* **71(2),** 487.
17. R. H. Mohiaddin, G. Z. Yang, P. Burger, D. N. Firmin, D. B. Longmore, *J. Comput. Assist. Tomogr.* **16(2),** 176 (1992).
18. G. R. Caputo, T. Masui, G. A. Gooding, J. M. Chang, C. B. Higgins, *Radiology* **182(2),** 387 (1992).
19. C. Kondo, G. R. Caputo, R. Semelka, E. Foster, A. Shimakawa, C. B. Higgins, *AJR* **157(1),** 9 (1991).
20. M. P. Marks, N. J. Pelc, M. R. Ross, D. R. Enzmann, *Radiology* **182(2),** 467 (1992).
21. J. M. Chang, K. Friese, G. R. Caputo, C. Kondo, C. B. Higgins, *J. Comput. Assist. Tomogr.* **15(3),** 418 (1991).
22. F. R. Korosec, C. A. Mistretta, P. A. Turski, *Magn. Reson. Med.* **24(2),** 221 (1992).
23. M. H. Buonocore, L. Gao, H. Bogren, A. Shimakawa, *in* "Book of Abstracts, 10th Annual Meeting, Society of Magnetic Resonance in Medicine, San Francisco, 1991," p 803.
24. T. E. Conturo, G. D. Smith, *Magn. Reson. Med.* **15,** 420 (1990).
25. N. J. Pelc, M. A. Bernstein, A. Shimakawa, G. H. Glover, *J. Magn. Reson. Imaging* **1(4),** 405 (1991).
26. T. E. Conturo, B. H. Robinson, *Magn. Reson. Med.* **25(2),** 233 (1992).
27. M. H. Buonocore, L. Gao, H. Bogren, *J. Magn. Reson. Imaging* **2,** 142 (1992).